ACS Catalysis

Research Article

pubs.acs.org/acscatalysis

Dye-Sensitized NiS_x Catalyst Decorated on Graphene for Highly Efficient Reduction of Water to Hydrogen under Visible Light Irradiation

Chao Kong,[†,‡] Shixiong Min,[†,‡] and Gongxuan Lu*[,†]

[†]State Key Laboratory for Oxo Synthesis and Selective Oxidation, Lanzhou Institute of Chemical Physics, Chinese Academy of Science, Lanzhou 730000, China

[‡]University of Chinese Academy of Science, Beijing 10080, China

Supporting Information

ABSTRACT: In this work, a highly active H_2 evolution NiS_x catalyst decorated on graphene (NiS_x/G) nanohybrid was prepared by an *in situ* chemical deposition method, in which nickel ion was first adsorbed onto graphene and subsequently reacted with sulfide ion to yield the NiS_x/G nanohybrid. The NiS_x/G catalyst exhibited activity for hydrogen generation 2-fold higher than that of pristine NiS_x under visible light irradiation. The highest quantum efficiency of 32.5% was reached at 430 nm when Eosin Y was used as a photosensitizer. In this system, graphene not only provided a large area and two-dimensional substrate for the confined growth of NiS_x but also greatly enhanced the transfer of photoelectrons from excited Eosin Y to the NiS_x cocatalyst because of its promotion of charge separation, leading to the great enhancement of photocatalytic hydrogen evolution.

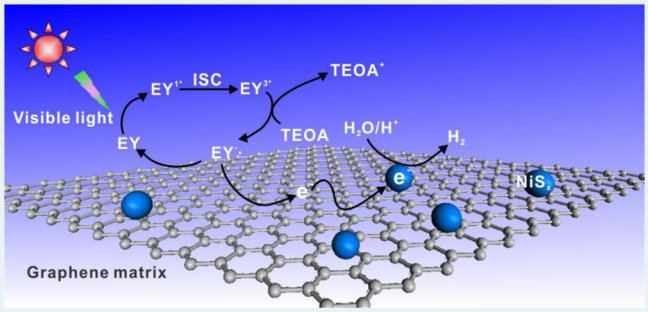

KEYWORDS: *NiS_x, graphene, dye, photocatalyst, visible light, hydrogen generation, sensitized*

1. INTRODUCTION

The generation of dye-sensitized photocatalytic hydrogen from water reduction is an important route for making the best use of solar light to produce clean and storable chemical energy because these catalysts absorb longer wavelength visible light that comprises a majority of the solar spectrum.[1−12] In this kind of catalyst, an excellent cocatalyst can work at highly active sites to reduce the overpotential of hydrogen evolution. Until now, photocatalysts loaded with noble metal Pt as a cocatalyst showed the high photocatalytic activity for the generation of hydrogen from water splitting;[13−16] however, the large-scale use of a Pt cocatalyst is difficult because of its scarcity.

Therefore, it is very important to develop cheaper systems by eliminating the use of expensive components, and recent studies indicate a number of non-noble metal catalysts are promising as substitutes for the Pt catalyst, including transition metal oxides,[17] transition metal hydroxides,[18] and transition metal sulfides.[19−21] Among these noble metal-free catalysts, nickel sulfide not only was cheap but also could replace Pt in the Pt/CdS photocatalytic H_2 generation system.[22] Zhang et al.[22] prepared highly active NiS/CdS photocatalytic material by a hydrothermal method for H_2 evolution using a lactic acid sacrificial solution, and the highest quantum efficiency at 420 nm was 51.3%. The NiS cocatalyst also exhibited photocatalytic H_2 generation activity higher than those of noble metals in enhancing the hydrogen evolution activity of the $CuGa_3S_5$ photocatalyst.[19] However, significantly improving the activity of the cocatalyst and developing low-cost and robust photocatalytic H_2 production cocatalysts remain challenging.

Recently, graphene has attracted tremendous interest in the photocatalytic reaction because of its remarkable physical, chemical, and electrical characteristics and large specific surface area.[23−25] The photoelectrical conversion and photocatalytic H_2 generation performance of semiconductors and cocatalysts (TiO_2, ZnO, CdS, CdSe, MoS_2, and Pt) could be improved significantly by loading on the surface of graphene.[26−39] Zhang et al.[32] revealed that the TiO_2 incorporated with graphene could induce the generation of hydrogen from water splitting under ultraviolet light. A $BiVO_4$-decorated graphene nanohybrid showed a remarkable enhancement in photoelectrochemical water splitting compared with that of pure $BiVO_4$ under visible light irradiation.[33] Min et al.[38] reported a MoS_2/graphene nanohybrid had a H_2 evolution efficiency higher than that of MoS_2 sensitized by xanthene dyes. In these systems, graphene could induce the transfer of photogenerated electrons from semiconductors or the excited dye to the cocatalyst via graphene because of its excellent properties, such as a high redox potential and excellent electron accepting and trans-

Received: May 20, 2014
Revised: July 11, 2014
Published: July 14, 2014

   dx.doi.org/10.1021/cs5006844 | ACS Catal. 2014, 4, 2763−2769

porting properties. The transfer of photogenerated electrons via graphene could effectively reduce the carrier recombination rate and significantly enhance the photocatalytic activity of hydrogen evolution.[26−31]

In this work, we report the facile preparation of a NiS_x-decorated graphene (NiS_x/G) cocatalyst by successive ionic absorption and reaction and its high activity of hydrogen generation sensitized by Eosin Y (EY) under visible light irradiation. Graphene could confine the growth of the NiS_x cocatalyst and produce more active sites and could also act as an excellent electron conductor to efficiently transfer photogenerated electrons from the excited dye to catalytic active sites of NiS_x, reducing the carrier recombination rate and improving the efficiency of photocatalytic hydrogen generation. Results showed that the photocatalytic hydrogen generation activity of NiS_x was enhanced by a factor of 2.04 after incorporation with graphene. The highest quantum yield of 32.5% was obtained at 430 nm. The NiS_x/G nanohybrid would be a promising substitute for precious metals in photocatalytic hydrogen generation systems.

2. EXPERIMENTAL SECTION

2.1. Synthesis of the NiS_x/G Nanohybrid and Measurement of Its Photocatalytic H_2 Evolution Activity and Apparent Quantum Efficiency (AQE). Graphite oxide (GO) and aqueous dispersions of graphene (3 mg mL^{-1}) were prepared by a modified Hummers method and the reduction of graphene oxide with sodium borohydride ($NaBH_4$) according to refs 37, 40, and 41, and more detailed information was given in the Supporting Information. The experimental apparatus and test methods were like those described in our previous study,[37] except for the following modifications. The synthesis of the NiS_x/G nanohybrid and measurement of its photocatalytic H_2 evolution activity were performed in a sealed Pyrex flask (150 mL) with a flat window (an efficient irradiation area of 13.2 cm^2) and a silicone rubber septum for sampling; 2 mL of these graphene suspensions (3 mg mL^{-1}) was dispersed in 100 mL of a triethanolamine (TEOA)/H_2O solution [10% (v/v)] with ultrasound treatment for ∼10 min, and the calculated amount of aqueous $Ni(NO_3)_2$, aqueous Na_2S (1:1 Ni:S molar ratio), and Eosin Y (EY, 1×10^{-3} mol L^{-1}) were added in the proper sequence while the sample was being stirred. Each addition was followed by magnetic stirring for 30 min. NiS_x was prepared in the absence of graphene by the same method. The method and measurement equipment of hydrogen and AQE were the same as those described in ref 37. The AQE was calculated with the following equation.

$$\text{AQE} = [(2 \times \text{the number of evolved hydrogen molecules}) / (\text{the number of incident photons})] \times 100\%$$

2.2. Electrochemical and Photoelectrochemical Measurements and Characterization. The experimental apparatus, electrode preparation methods, and sample characterization were the same as those reported previously[37] (see parts 4−6 of the Supporting Information for more details).

3. RESULTS AND DISCUSSION

The mechanism of formation of the NiS_x/G nanohybrid is illustrated in Scheme 1. The graphene suspension was ultrasonicated in a TEOA solution to give a homogeneous graphene dispersion, and then $Ni(NO_3)_2$ and Na_2S solutions were added successively to the suspension, in which Ni^{2+} was

Scheme 1. Formation of NiS_x/G by the *in Situ* Chemical Deposition Method

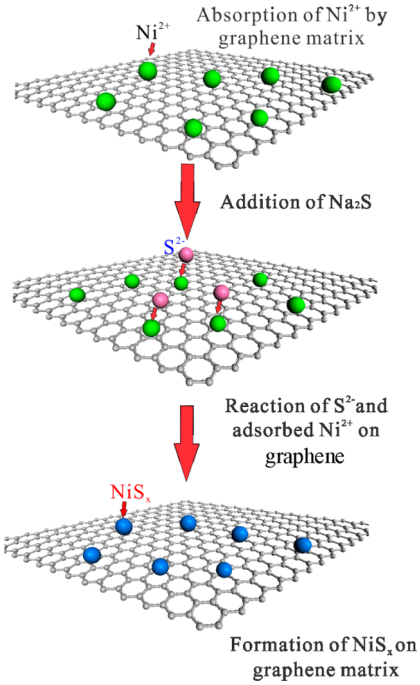

first adsorbed onto graphene sheets through coulomb forces because of its negative charge and then reacted with S^{2-} to form NiS_x nanoparticles, resulting in the NiS_x/G nanohybrid. The morphologies of NiS_x and NiS_x/G were characterized by transmission electron microscopy (TEM). As noted in panels A and B of Figure 1, NiS_x nanoparticles tightly adhered to the surface of graphene with particle sizes of 20−40 nm, while pristine NiS_x had a networklike structure similar to that of nickel sulfide prepared by Zhang et al.[21] These results suggest that graphene sheets act as a confined substrate to control nucleation and following the growth of NiS_x nanoparticles by fixing the Ni^{2+} position, which led to the different morphology of NiS_x nanoparticles. The high-resolution TEM (HRTEM) image of NiS_x/G shown in Figure 1C reveals that NiS_x nanoparticles on graphene were crystalline. Lattice spacings of 0.24 and 0.34 nm could be indexed to the (400) and (220) planes, respectively, of hexagonal Ni_3S_4, and the interplanar spacing of 0.41 nm belonged to the (010) plane of hexagonal Ni_3S_2.

Figure 2A shows the X-ray diffraction (XRD) patterns of the NiS_x/G nanohybrid and NiS_x. The diffraction peaks at 2θ values of 21.8° and 44.0° were assigned to the (010) and (020) planes, respectively, of hexagonal Ni_3S_2 (JCPDS Card No. 73-0698), while the peak at a 2θ value of 31.7° belonged to the (110) plane of hexagonal Ni_3S_2 and the (311) plane of cubic Ni_3S_4 (JCPDS Card No. 47-1739). The appearance of cubic phase Ni_3S_4 in NiS_x/G could also be identified by the strong diffraction peak at a 2θ value of 26.1°, which was assigned to the (220) plane of cubic Ni_3S_4. These results were consistent with the HRTEM characterization and indicated the graphene could facilitate the growth of the (220) planes of Ni_3S_4 because of the confined function of graphene. In addition, a broad peak centered at a 2θ value of 22.8° belonged to graphene in the NiS_x/G nanohybrid, which confirmed a random packing of graphene because of the low content of NiS_x,[37] and might overlap with some diffraction peak of NiS_x. These results

dx.doi.org/10.1021/cs5006844 | ACS Catal. 2014, 4, 2763−2769

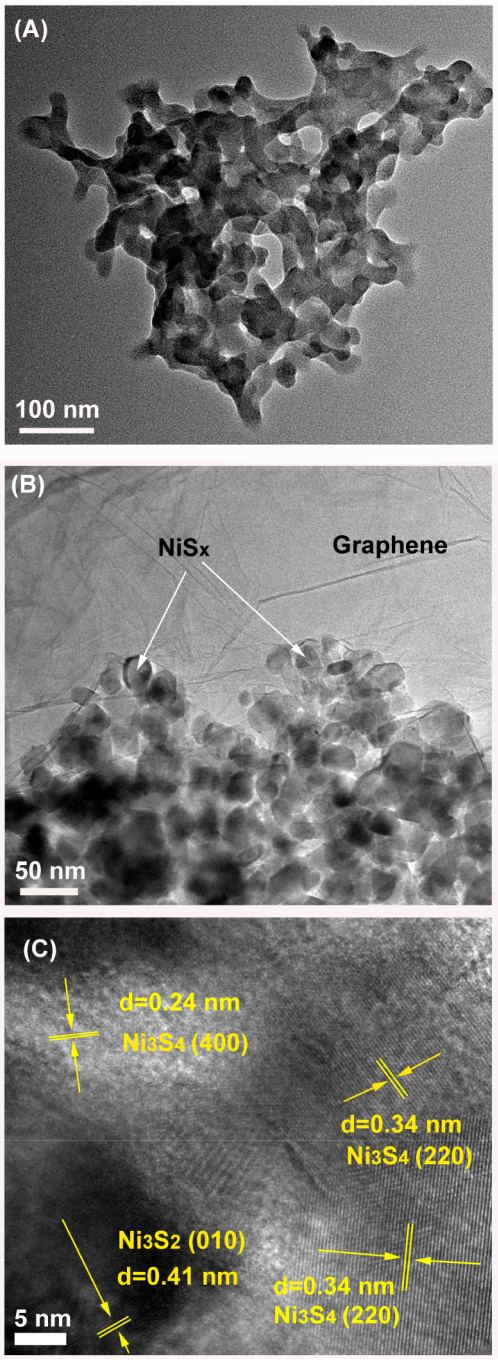

Figure 1. (A) TEM images of NiS_x. (B and C) TEM and HRTEM images, respectively, of the NiS_x/G nanohybrid.

indicate that nickel sulfide species for both samples should exist as mixed phases of hexagonal Ni_3S_2 and cubic Ni_3S_4.

NiS_x and the NiS_x/G nanohybrid were further characterized by X-ray photoelectron spectroscopy (XPS). Figure 2B shows that both NiS_x and NiS_x/G consisted of Ni, S, C, and O. XPS analysis showed the Ni:S molar ratio was 0.97 in NiS_x/G and 0.84 in NiS_x. The S 2p XPS spectra of NiS_x/G in Figure 2C exhibit the higher binding energies of S 2p (163.2 eV) compared to that of NiS_x (162.2 eV),[42−44] and the Ni $2p_{3/2}$ spectra in Figure 2D show that the binding energies of Ni $2p_{3/2}$ in NiS_x/G occurred at 854.2 eV, which was slightly higher than that of NiS_x (852.9 eV).[44−47] These results indicate that NiS_x had a strong interaction with graphene in NiS_x/G, which was from the coelectron cloud formed between NiS_x and the adjacent carbon layer.[48,49] The coelectron cloud between NiS_x and graphene sheets could significantly improve the electronic conductivity of NiS_x/G, which helped the transfer of photogenerated electrons from graphene to NiS_x in the process of photocatalytic hydrogen generation.[38] In Figure 2C, the peak at approximately 168.1 eV indicates that SO_4^{2-} exists in NiS_x and NiS_x/G. These peaks observed at 855.3 and 855.8 eV in Figure 2D indicate that a trace of Ni_2O_3 formed.[50] These four peaks at 860.2, 860.0, 878.2, and 877.8 eV were assigned to the satellites of Ni $2p_{3/2}$ and Ni $2p_{1/2}$, respectively.

Figure 3A shows the generation of photocatalytic H_2 over graphene, NiS_x, Pt, and NiS_x/G cocatalysts when EY was used as sensitizer under visible light irradiation. As shown in Figure 3A, the introduction of graphene and NiS_x was crucial in enhancing the photocatalytic H_2 evolution activity. In the absence of NiS_x nanoparticles, only 3.64 μmol of H_2 was produced in the EY-graphene system, which indicated that graphene was a low-H_2 generation active cocatalyst probably because it had a high electron affinity and unfavorable hydrogenated surfaces.[37−39] In the EY-NiS_x system, the rate of H_2 generation was 34.2 μmol h^{-1} in the beginning, reached the maximum (~109.9 μmol h^{-1}) after irradiation for 0.5 h, and decreased gradually with an increase in irradiation time; 293.5 μmol of H_2 was generated within 5.5 h of irradiation, and the average rate was ~53.4 μmol h^{-1}. The result also shows that NiS_x was a highly active H_2 generation cocatalyst in dye-sensitized photocatalytic hydrogen generation. The NiS_x/G nanohybrid showed photocatalytic activity higher than those of pristine NiS_x and Pt (see experimental details in the Supporting Information), and the amount of H_2 evolved was 599.1 μmol in 5.5 h when the mass fraction of NiS_x was 46.7% in relation to graphene, which was 2.04 times higher than that of NiS_x under the same experimental conditions. The photocatalytic H_2 evolution activity of NiS_x/G with different NiS_x:graphene weight ratios was also investigated. As shown in Figure 3B, the amount of H_2 evolved over NiS_x/G was increased with an increase in the NiS_x:graphene weight ratio and achieved the maximum when the NiS_x:graphene weight ratio was ~46.7%. Further increases led to a slight reduction in the activity of the NiS_x/G nanohybrid. This might be ascribed to the change in the morphology of NiS_x and the reduction of the graphene absorption site to EY in NiS_x/G by the deposition of excessive NiS_x. When the NiS_x:graphene weight ratio was ~77.6%, the photocatalytic H_2 evolution activity had slightly increased compared to a value of 62%.

To investigate the wavelength dependence of photocatalytic H_2 evolution, the apparent quantum efficiencies (AQEs) of EY-NiS_x, EY-Pt, and EY-NiS_x/G systems were examined over a wide visible light range of 430−550 nm. As shown in Figure 4A, the maximal AQE of the EY-Pt system located at 430 nm was 39.7%. The EY-NiS_x/G system showed an AQE higher than that of the EY-NiS_x system in the experimental wavelength range, and the highest AQE of 32.5% was obtained at 430 nm, which was shorter than the highest absorption wavelength of EY (518 nm) in the visible light range. This result might be due to its higher absorption at 430 nm and the higher potential of photons because the EY-NiS_x/G system had an absorbance higher than that of EY in the short wavelength region (see Figure S2 of the Supporting Information). Furthermore, the stability of the EY-NiS_x/G system was examined, and the results are shown in Figure 4B. The amount of H_2 production in the second run was around 17% of that of the first run, and that of

dx.doi.org/10.1021/cs5006844 | ACS Catal. 2014, 4, 2763−2769

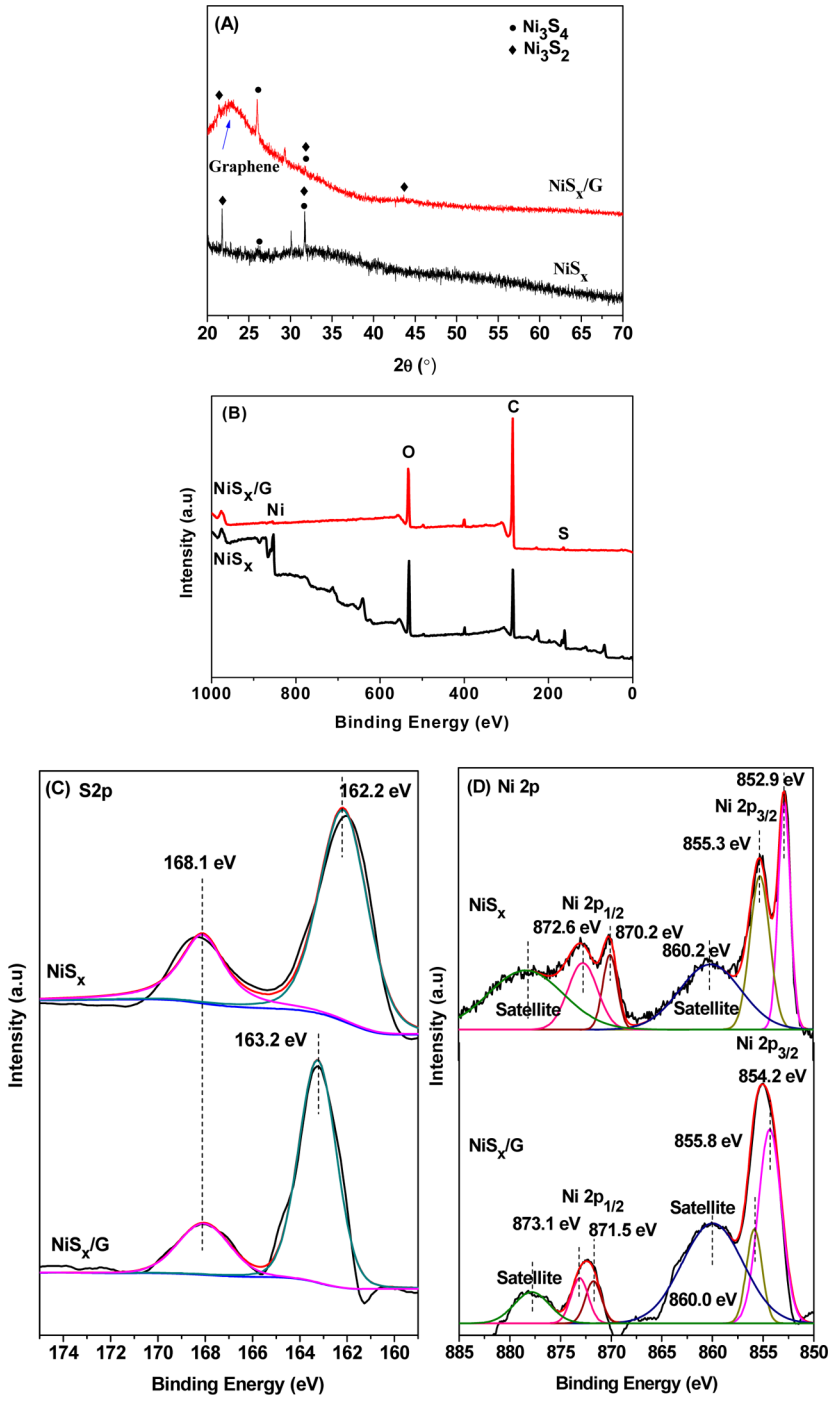

Figure 2. (A) X-ray diffraction patterns of NiS_x and the NiS_x/G nanohybrid. (B) X-ray photoelectron spectroscopy survey spectra of NiS_x and the NiS_x/G nanohybrid. (C) S 2p and (D) Ni 2p scan spectra of NiS_x and the NiS_x/G nanohybrid.

the third run reached 33.6% when the fresh EY was supplemented. A decline in the photocatalytic activity of NiS_x/G was due to decomposition of both the photosensitizer and the sacrificial donor during photolysis.[38] The H_2 evolution activity of EY-NiS_x/G could be revived to 42.9% by the concurrent addition of EY and TEOA in the fourth run. The results show that the NiS_x/G cocatalyst was relatively stable during photocatalytic hydrogen generation.

The proposed mechanism of photocatalytic H_2 generation in EY-NiS_x/G system is depicted in Scheme 2. A certain amount of EY might be adsorbed on the surface of graphene in the NiS_x/G nanohybrid because of the noncovalent $\pi-\pi$ interaction of graphene sheets and EY,[38] and the adsorbed EY might gain a photon and produce singlet excited state $EY^{1}*$ under visible light and subsequently produce a lowest-lying triplet excited state $EY^{3}*$ via an intersystem crossing (ISC). $EY^{3}*$ might be reductively quenched by a sacrificial donor TEOA to produce $EY^{-\bullet}$.[51−53] Those $EY^{-\bullet}$ species might preferentially transfer their electrons to graphene, leading to the spatial separation of photogenerated charges.[37−39] These electrons on the surface of graphene sheets could be transferred to the suitable Ni 3d and S 3p hybrid orbital of the NiS_x cocatalyst, and the reduced valence state of Ni could facilitate the proton reduction for H_2 generation.[21] In the absence of

dx.doi.org/10.1021/cs5006844 | ACS Catal. 2014, 4, 2763−2769

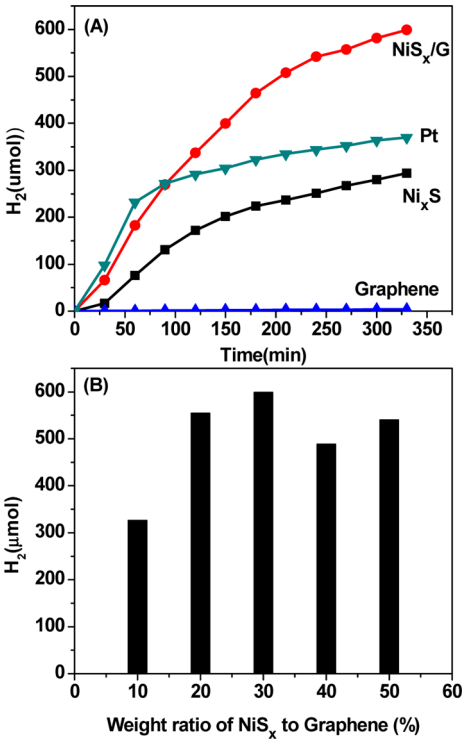

Figure 3. (A) Time courses of hydrogen evolution over EY-graphene, EY-NiS_x, EY-Pt, and EY-NiS_x/G photocatalysts from EY (1.0×10^{-3} mol L^{-1})-photosensitized systems in 100 mL of a 10% (v/v) aqueous TEOA solution (pH 7) under visible light irradiation ($\lambda \geq 420$ nm). The NiS_x:graphene weight ratio is 46.7% in NiS_x/G. (B) Comparison of the photocatalytic activity of NiS_x/G with different NiS_x:graphene weight ratios for the H_2 production photosensitized by EY (1.0×10^{-3} mol L^{-1}) in a 10% (v/v) aqueous TEOA solution (pH 7) under visible light irradiation ($\lambda \geq 420$ nm). The system was irradiated with a 300 W Xe lamp with a cutoff filter of 420 nm. The amount of graphene was 6 mg.

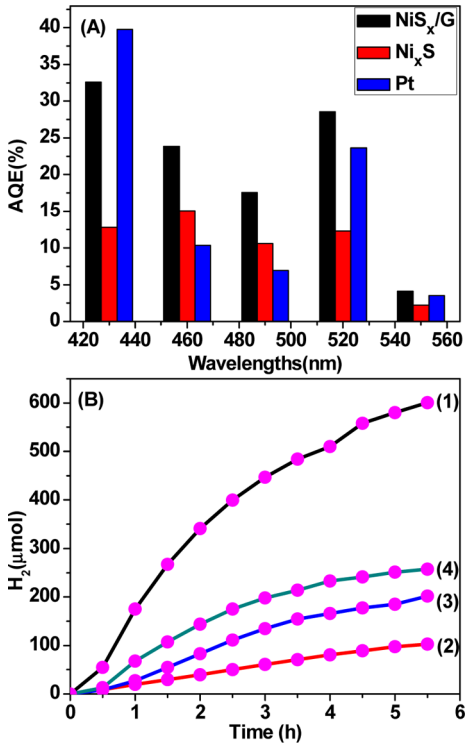

Figure 4. (A) Apparent quantum efficiencies (AQEs) of H_2 evolution for EY (1.0×10^{-3} mol L^{-1})-photosensitized systems catalyzed by NiS_x (2.8 mg), Pt (2.8 mg), and the NiS_x/G nanohybrid (NiS_x, 2.8 mg; graphene, 6 mg) in 100 mL of a 10% (v/v) aqueous TEOA solution under light irradiation with different wavelengths. The system was irradiated with a 300 W Xe lamp with a cutoff filter of 420 nm and a bandpass filter. During the AQE tests, the reaction solutions were irradiated under $\lambda \geq 420$ nm for 30 min before switching to bandpass filters for the AQE on the H_2 production for the subsequent 2 h. (B) Stability test of H_2 evolution over the EY (1.0×10^{-3} mol L^{-1})-sensitized NiS_x/G catalyst (NiS_x, 2.8 mg; graphene, 6 mg) in 100 mL of a 10% (v/v) aqueous TEOA solution under visible light irradiation ($\lambda \geq 420$ nm). The reaction was continued for 22 h, with evacuation every 5.5 h: (1) first run, (2) evacuation, (3) addition of EY and evacuation, and (4) collection of NiS_x/G by centrifugation of the reaction mixture. After being washed thoroughly several times using DI water, the recycled NiS_x/G was mixed with a TEOA solution and fresh EY and evacuated. The system was irradiated with a 300 W Xe lamp with an optical cutoff filter of 420 nm.

graphene, those highly reductive $EY^{-\bullet}$ species might recombine rapidly with $TEOA^+$ or dye species, leading to the low activity of photocatalytic H_2 evolution. Therefore, graphene could enhance the catalytic H_2 evolution activity of the NiS_x/G nanohybrid by prolonging the lifetime of photogenerated electrons and consequently improving the charge separation efficiency.

To prove the important role of graphene in facilitating the transfer of photogenerated electrons to improve the NiS_x/G photocatalytic activity, the photoluminescence quenching of EY in the presence of the NiS_x/G nanohybrid and NiS_x was further examined, as shown in Figure 5A. The excitation wavelength was 505 nm. The aqueous EY solution had an intensive emission peak located at 540 nm caused by its strong recombination of excited charge pairs by exciting light.[37,53] As NiS_x/G and NiS_x were introduced into the aqueous EY solution, there was a significant decrease in the peak intensity of EY emission, and the quenching efficiency of NiS_x/G (~67.5%) was significantly higher than that of NiS_x (~14.3%); meanwhile, slight red (~1 nm) and blue (~3 nm) shifts of the emission peak center were also observed due to the presence of NiS_x and NiS_x/G, respectively, which could be mainly ascribed to the noncovalent $\pi-\pi$ interaction of graphene or NiS_x with EY and the interfacial electron transfer from the attached EY* to the graphene sheets or NiS_x.[34,54] In addition, the fluorescence lifetime of EY in the presence of NiS_x or NiS_x/G was investigated to probe the excited charge transfer. The fluorescence lifetimes were obtained by fitting the decay profiles with one exponential term and two exponential terms,

Scheme 2. Proposed Photocatalytic Mechanism for Hydrogen Evolution over the EY-NiS_x/G Photocatalyst under Visible Light Irradiation

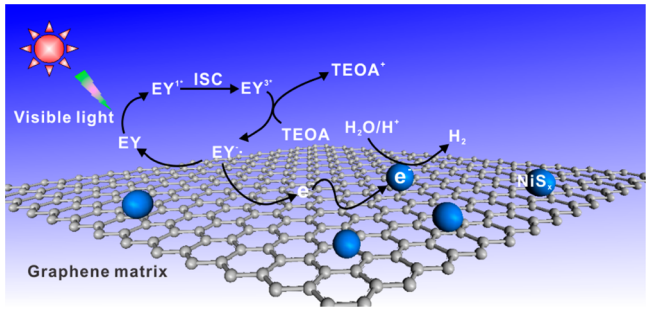

dx.doi.org/10.1021/cs5006844 | ACS Catal. 2014, 4, 2763−2769

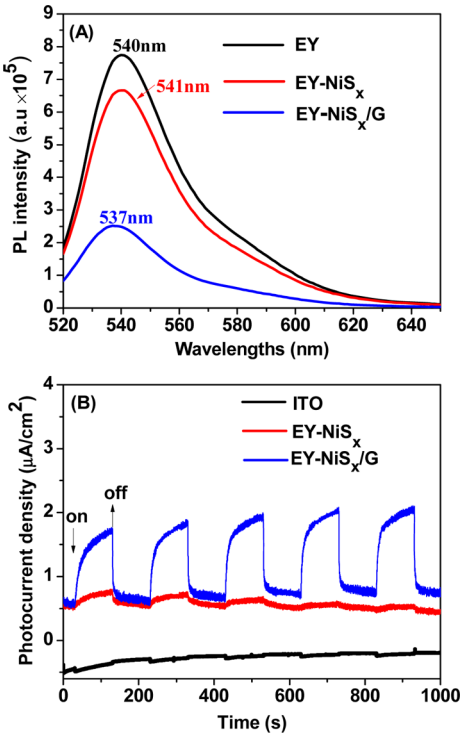

Figure 5. (A) Photoluminescence quenching (excitation wavelength of 505 nm) of EY (1.0×10^{-5} mol L^{-1}) by NiS_x and NiS_x/G in a 10% (v/v) TEOA solution. The weight concentration of NiS_x is 0.073 mg mL^{-1} in EY-NiS_x. The weight concentration of NiS_x/G is 0.073 mg mL^{-1} in EY-NiS_x/G (NiS_x:graphene weight ratio of 46.7%). (B) Transient photocurrent−time profiles of EY-sensitized NiS_x and NiS_x/G coated on ITO glass in a mixed solution of 10% (v/v) TEOA and Na_2SO_4 (0.1 mol/L) at pH 7 under visible light irradiation (≥420 nm).

respectively. In Table 1, the fluorescence lifetime of EY was 0.311 ns, which changed slightly in the presence of NiS_x (0.349 ns). In the EY-NiS_x/G system, the graphene-bound EY and the unbound form coexisted and the fluorescence lifetime of long decay components was 1.84 ns.[38] These results reveal that the lifetime of the singlet excited EY^{1}* could be prolonged in EY-NiS_x/G systems. The long lifetime of EY^{1}* could greatly facilitate the production of EY^{3}* via the intersystem crossing (ISC), which was beneficial for the generation of $EY^{-\bullet}$.

Table 1. Decay Parameters of EY in the Presence of NiS_x and NiS_x/G[a]

system	lifetime (ns)	pre-exponential factor A (%)	average lifetime $\langle\tau\rangle$ (ns)	χ^2
EY	τ = 0.304	A = 50	0.304	0.9969
EY-NiS_x	τ = 0.349	A = 50	0.349	0.9998
EY-NiS_x/G	τ_1 = 0.204, τ_2 = 1.84	A_1 = 94.7, A_2 = 5.3	0.752	1.0001

[a]The concentrations of dyes and catalysts were 1×10^{-4} mol/L and 0.005 mg/mL, respectively. A single-exponential fit was used for EY and EY-NiS_x. A double-exponential fit was used for EY-NiS_x/G. The average lifetime was determined according to the reported method.[55].

Moreover, the transient photocurrent responses of EY-NiS_x/ITO and EY-NiS_x/G/ITO electrodes were investigated and are shown in Figure 5B. In Figure 5B, the EY-NiS_x/G/ITO electrode exhibited a noticeable improvement in its photocurrent relative to that of EY-NiS_x/ITO. These results reveal that the transfer of electrons from $EY^{-\bullet}$ to NiS_x/G is fast as well as that to the interface of ITO glass and NiS_x/G due to the presence of graphene, while the $EY^{-\bullet}$ species formed in the solution continuously via the reductive quenching of EY^{3}* in the presence of TEOA. Therefore, in the EY-NiS_x/G photocatalytic system, graphene functioned as an excellent electron acceptor and transporter to efficiently prolong the lifetime of the photogenerated electon and consequently enhance the H_2 generation of the NiS_x/G nanohybrid under visible light.

To provide further evidence that graphene was important for improving the photocatalytic H_2 evolution activity of the NiS_x/G nanohybrid, the electrochemical H_2 generation activities of NiS_x/ITO and NiS_x/G/ITO electrodes were investigated by the linear sweep voltammetry (LSV) technique as shown in Figure 6. The cathodic current of the bare ITO electrode was still low with an increase in the applied potential. The enhancement of the cathodic current of the NiS_x/ITO electrode at the same potentials revealed that NiS_x was a remarkable electrocatalyst that could efficiently facilitate the reduction of proton.[56] The cathodic current of NiS_x/G/ITO electrodes was significantly improved beyond −0.7 V, which indicated that graphene of the NiS_x/G nanohybrid could synergistically promote the reduction of protons to generate H_2.

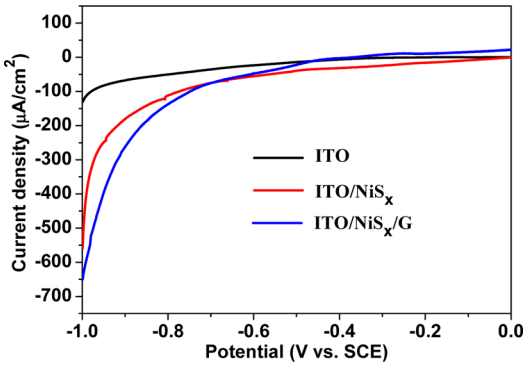

Figure 6. LSV curves of bare ITO glass and NiS_x- and NiS_x/G-coated ITO electrodes in a mixed solution of 10% (v/v) TEOA and 0.1 mol/L Na_2SO_4 at pH 7. The scan rate was 1 mV s^{-1}.

4. CONCLUSION

In summary, we prepared a highly active H_2 evolution catalyst of NiS_x-decorated graphene (NiS_x/G) nanohybrids by *in situ* chemical deposition NiS_x on graphene in solution, which was a simple and scalable process and could easily be adapted for a large scale. The NiS_x/G catalyst exhibited an activity for hydrogen evolution higher than that of pristine NiS_x under visible light irradiation ($\lambda \geq 420$ nm). The highest quantum efficiency of 32.5% at 430 nm was reached when the NiS_x:graphene weight ratio was 46.7% in the nanohybrid. The graphene of the NiS_x/G nanohybrid could confine the growth of the NiS_x cocatalyst to expose more active sites and act as an excellent electron conductor to efficiently transfer photogenerated electrons from the excited dye to catalytic active sites of NiS_x, thereby reducing the carrier recombination rate and improving the efficiency of photocatalytic hydrogen generation. The NiS_x/G nanohybrid represents a highly active

dx.doi.org/10.1021/cs5006844 | ACS Catal. 2014, 4, 2763−2769

cocatalyst that is a promising substitute for precious metals in the photocatalytic hydrogen generation system.

■ ASSOCIATED CONTENT

Supporting Information

Additional information as noted in the text. This material is available free of charge via the Internet at http://pubs.acs.org.

■ AUTHOR INFORMATION

Corresponding Author

*E-mail: gxlu@lzb.ac.cn. Telephone: +86-931-4968 178.

Notes

The authors declare no competing financial interest.

■ ACKNOWLEDGMENTS

We are grateful for the support by the 973 and 863 Programs of the Department of Sciences and Technology of China (2013CB632404 and 2012AA051501) and the NSFC of China (Grant 21173242).

■ REFERENCES

(1) Zhang, W.; Hong, J. D.; Zheng, J. W.; Huang, Z. Y.; Zhou, J. R.; Xu, R. *J. Am. Chem. Soc.* **2011**, *133*, 20680−20683.
(2) Du, P. W.; Schneider, J.; Jarosz, P.; Eisenberg, R. *J. Am. Chem. Soc.* **2006**, *128*, 7726−7727.
(3) Zhang, X. J.; Jin, Z. L.; Li, Y. X.; Li, S. B.; Lu, G. X. *J. Phys. Chem. C* **2009**, *113*, 2630−2635.
(4) Zhang, P.; Wang, M.; Li, C. X.; Li, X. Q.; Dong, J. F.; Sun, L. C. *Chem. Commun.* . **2010**, *46*, 8806−8808.
(5) Du, P. W.; Eisenberg, R. *Energy Environ. Sci.* **2012**, *5*, 6012−6021.
(6) Li, Q.; Jin, Z.; Peng, Z.; Li, Y.; Li, S.; Lu, G. *J. Phys. Chem. C* **2007**, *111*, 8237−8241.
(7) Abe, R.; Hara, K.; Sayama, K.; Domen, K. *J. Photochem. Photobiol., A* **2000**, *137*, 63−69.
(8) Li, B.; Lu, G. *Fenzi Cuihua* **2013**, *27*, 181−191.
(9) Li, Q.; Chen, L.; Lu, G. *J. Phys. Chem. C* **2007**, *111*, 11494−11499.
(10) Youngblood, W. J.; Lee, S-H. A.; Maeda, K.; Mallouk, T. E. *Acc. Chem. Res.* **2009**, *42*, 1966−1973.
(11) Yum, J. H.; Jang, S. R.; Walter, P.; Geiger, T.; Nuesch, F.; Kim, S.; Ko, J.; Gratzel, M.; Nazeeruddin, M. K. *Chem. Commun.* **2007**, 4680−4682.
(12) Zhang, W.; Hong, J. D.; Zheng, J. W.; Huang, Z. Y.; Zhou, J. R.; Xu, R. *J. Am. Chem. Soc.* **2011**, *133*, 20680−20683.
(13) Walter, M. G.; Warren, E. L.; McKone, J. R.; Boettcher, S. W.; Mi, Q.; Santori, E. A.; Lewis, N. S. *Chem. Rev.* **2010**, *110*, 6446−6473.
(14) Bao, N. Z.; Shen, L. M.; Takata, T.; Domen, K. *Chem. Mater.* **2008**, *20*, 110−117.
(15) Yan, H.; Yang, J.; Ma, G.; Wu, G.; Zong, X.; Lei, Z.; Shi, J.; Li, C. *J. Catal.* **2009**, *266*, 165−168.
(16) Zhou, P.; Zhao, C.; Dong, W.; Lu, G. *Fenzi Cuihua* **2012**, *26*, 265−275.
(17) Thaminimulla, C. T. K.; Takata, T.; Hara, M.; Kondo, J. N.; Domen, K. *J. Catal.* **2000**, *196*, 362−365.
(18) Yu, J. G.; Ran, J. R. *Energy Environ. Sci.* **2011**, *4*, 1364−1371.
(19) Tabata, M.; Maeda, K.; Ishihara, T.; Minegishi, T.; Takata, T.; Domen, K. *J. Phys. Chem. C* **2010**, *114*, 11215−11220.
(20) Zhang, L.; Tian, B. Z.; Chen, F.; Zhang, J. L. *Int. J. Hydrogen Energy* **2012**, *37*, 17060−17067.
(21) Zhang, W.; Xu, R. *Int. J. Hydrogen Energy* **2012**, *37*, 17899−17909.
(22) Zhang, W.; Wang, Y. B.; Wang, Z.; Zhong, Z. Y.; Xu, R. *Chem. Commun.* **2010**, *46*, 7631−7633.
(23) Geim, A. K.; Novoselov, K. S. *Nat. Mater.* **2007**, *6*, 183−191.
(24) Geim, A. K. *Science* **2009**, *324*, 1530−1534.
(25) Allen, M. J.; Tung, V. C.; Kaner, R. B. *Chem. Rev.* **2010**, *110*, 132−145.
(26) Xiong, Z.; Zhang, L.; Ma, J.; Zhao, X. *Chem. Commun.* **2010**, *46*, 6099−6101.
(27) Cao, A.; Liu, Z.; Chu, S.; Wu, M.; Ye, Z.; Cai, Z.; Chang, Y.; Wang, S.; Gong, Q.; Liu, Y. *Adv. Mater.* **2010**, *22*, 103−106.
(28) Geng, X. M.; Niu, L.; Xing, Z. Y.; Song, R. S.; Liu, G. T.; Sun, M. T.; Cheng, G. S.; Zhong, H. J.; Liu, Z. H.; Zhang, H. J.; Sun, L. F.; Xu, H. X.; Lu, L.; Liu, L. W. *Adv. Mater.* **2010**, *22*, 638−642.
(29) Lin, Y.; Zhang, K.; Chen, W.; Liu, Y.; Geng, Z.; Zeng, J.; Pan, N.; Yan, L.; Wang, X.; Hou, J. G. *ACS Nano* **2010**, *4*, 3033−3038.
(30) Guo, C.; Yang, H.; Sheng, Z.; Lu, Z.; Song, Q.; Li, C. *Angew. Chem., Int. Ed.* **2010**, *49*, 3014−3017.
(31) Kim, S. R.; Parvez, M. K.; Chhowalla, M. *Chem. Phys. Lett.* **2009**, *483*, 124−127.
(32) Zhang, X.; Li, H.; Cui, X.; Lin, Y. *J. Mater. Chem.* **2010**, *20*, 2801−2806.
(33) Ng, Y. H.; Iwase, A.; Kudo, A.; Amal, R. *J. Phys. Chem. Lett.* **2010**, *1*, 2607−2612.
(34) Du, J.; Zhang, H.; Lv, X.; Li, Y.; Wang, Y.; Li, J. *ACS Nano* **2010**, *4*, 380−386.
(35) Chen, C.; Cai, W.; Long, M.; Zhou, B.; Wu, Y.; Wu, D.; Feng, Y. *ACS Nano* **2010**, *4*, 6425−6432.
(36) Xu, T. G.; Zhang, L. W.; Cheng, H. Y.; Zhu, Y. F. *Appl. Catal., B* **2011**, *101*, 382−387.
(37) Min, S.; Lu, G. *J. Phys. Chem. C* **2011**, *115*, 13938−13945.
(38) Min, S.; Lu, G. *J. Phys. Chem. C* **2012**, *116*, 25415−25424.
(39) Min, S.; Lu, G. *Int. J. Hydrogen Energy* **2012**, *37*, 10564−10574.
(40) Hummers, W. S.; Offeman, R. E. *J. Am. Chem. Soc.* **1958**, *80*, 1339.
(41) Kovtyukhova, N. I.; Ollivier, P. J.; Martin, B. R.; Mallouk, T. E.; Chizhik, S. A.; Buzaneva, E. V.; Gorchinskiy, A. D. *Chem. Mater.* **1999**, *11*, 771−778.
(42) Wanger, C. D.; Taylor, J. A. *J. Electron Spectrosc. Relat. Phenom.* **1980**, *20*, 83−93.
(43) Matoba, M.; Anzai, S.; Fujimori, A. *J. Phys. Soc. Jpn.* **1991**, *6*, 4230−4244.
(44) Shalvoy, R. B.; Reucroft, P. J. *J. Vac. Sci. Technol.* **1979**, *16*, 567−570.
(45) Chandramohan, S.; Kang, J. H.; Ryu, B. D.; Yang, J. H.; Kim, S.; Kim, H.; Park, J. B.; Kim, T. Y.; Cho, B. J.; Suh, E. K.; Hong, C. H. *ACS Appl. Mater. Interfaces* **2013**, *5*, 958−964.
(46) Loechel, B. P.; Strehblow, H. H. *J. Electrochem. Soc.* **1984**, *131*, 713−723.
(47) Bianchi, D.; Borcar, S.; Teule-Gay, F.; Bennett, C. O. *J. Catal.* **1983**, *82*, 424−456.
(48) Lachkar, A.; Selmani, A.; Sacher, E. *Synth. Met.* **1995**, *72*, 73−80.
(49) Tolman, C. A.; Riggs, W. M.; Linn, W. J.; King, C. M.; Wendt, R. C. *Inorg. Chem.* **1973**, *12*, 2270−2278.
(50) Zhao, W.; Ma, W. H.; Chen, C. C.; Zhao, J. C.; Shuai, Z. G. *J. Am. Chem. Soc.* **2004**, *126*, 4782−4783.
(51) Shimidzu, T.; Iyoda, T.; Koide, Y. *J. Am. Chem. Soc.* **1985**, *107*, 35−41.
(52) Lazarides, T.; McCormick, T.; Du, P. W.; Luo, G. G.; Lindley, B.; Eisenberg, R. *J. Am. Chem. Soc.* **2009**, *131*, 9192−9194.
(53) De, S.; Das, S.; Girigoswami, A. *Spectrochim. Acta, Part A* **2005**, *61*, 1821−1833.
(54) Liu, Y.; Liu, C.; Liu, Y. *Appl. Surf. Sci.* **2011**, *257*, 5513−5518.
(55) Williams, G.; Kamat, P. V. *Langmuir* **2009**, *25*, 13869−13873.
(56) Zong, X.; Wu, G. P.; Yan, H. J.; Ma, G. J.; Shi, J. Y.; Wen, F. Y.; Wang, L.; Li, C. *J. Phys. Chem. C* **2010**, *114*, 1963−1968.